JOURNAL OF MATERIALS SCIENCE 33 (1998) 2431–2440

Processes involved during the production of Fe–W–Mo alloys by powder metallurgy

S. E. BARAMA, A. HARABI
Research Unit in Materials Physics and Applications, University of Constantine, Constantine 25000, Algeria

G. CIZERON
Laboratoire de structure des matériaux métalliques, Université de Paris-sud, Centre d'Orsay, 91405 Orsay, France

Sintering of Fe–W–Mo systems under a dynamic atmosphere of argon has been studied by different experimental techniques, including dilatometric trials, X-ray diffraction, optical microscopy and electron probe microanalysis. It has been found that sintering at 1300 °C for only 10 min allows compacts to be obtained with a relative density close to 80%. The results also show an improvement in the final density by molybdenum addition. On the other hand, the structure of the sintered samples was, mainly, constituted of a soft matrix of $(Fe–M)_\alpha$ solid solutions ($\sim 300\,H_v$) in which hard intermetallic compounds ($\sim 1200\,H_v$) are dispersed. Furthermore, perturbing expansions have been observed during the sintering cycle. The first expansion occurred at about 620 °C as a consequence of a Kirkendall effect. The second one arose at about 890 °C in relation to Fe_7M_6 (where M is tungsten or molybdenum) formation. The latter expansion occurred at about 1200 °C as a consequence of an increase in tungsten diffusion from indiffused areas to $(Fe–M)_a$ solid solutions and intermetallic compounds.

1. Introduction

The structure of metallic components, destined for wear applications, must be essentially constituted of hard phases dispersed in a tougher matrix. Such structure actually permits grooving and local welding to be reduced. In the case of the conventional wear material, the hard phases are generally carbide precipitates dispersed throughout high-speed steel (HSS) matrices. However, certain problems may occur when mechanical parts are produced from such materials. The more important of them are related to the coarsening and also segregation of carbides to the network carbides obtained after cooling. Several solutions have been proposed to avoid these problems. Among them the realization of mechanical parts by the powder metallurgy processing route has generated considerable interest in research investigations [1–4]. Prealloyed high-speed steel (HSS) powders with added hard ceramic particles are frequently used as starting materials in these investigations. In spite of the promising results obtained with such materials, many difficulties remain, however, without solutions. These difficulties are mainly related to the fact that certain types of ceramics dissolved completely in the metallic matrices at the sintering temperatures [5–8]. On the contrary, other types of added ceramics did not react sufficiently with the metallic matrices and hence were not well wetted after sintering [5, 9]. Additionally, subsequent heat treatments are always necessary to achieve a high densification of the as-processed parts. Consequently, a high expenditure is often required for their production [10–12].

In the present investigation, production of Fe–W–Mo alloys destined for wear utilization by the powder metallurgy processing route, was attempted. The choice of these materials was dictated by the fact that additions of tungsten or molybdenum to iron permit hard intermetallic compounds of Fe_2M and Fe_7M_6 stoichiometry (where M is tungsten or molybdenum) to be obtained dispersed in a tougher $(Fe–M)_\alpha$ matrix [13, 14]. Such alloys must constitute, therefore, another alternative for wear materials. Nevertheless, their production by the conventional processing route is not easy, because of the high melting points of both tungsten and molybdenum and their great difference from that of iron. The powder metallurgy route may constitute, in these conditions, the appropriate alternative processing for their production.

2. Experimental procedure

Carbonyl iron supplied by Baudier, reduced molybdenum and reduced tungsten (both supplied by Metafram) were used as starting powders. The average sizes of the three types of powders were 5.0, 5.0 and 0.5 μm, respectively. Various mixtures were prepared in a Turbula-type apparatus for 2 h, by mixing the three types

of powders into the required weight percentages. Green compacts were then prepared by pressing mixtures in floating dies at 600 MPa. Conventional sintering of compacts was carried out, under a dynamic atmosphere of argon, at 1300 °C for 10 min. The heating rate of the samples from room temperature to the sintering temperature was 10 °C min^{-1}, while the cooling of compacts was carried out in the furnace.

In order to approach the sintering mechanisms of these materials, shrinkage of Fe–xW–yMo agglomerates (where $15\,wt\,\% \leqslant x \leqslant 30\,wt\,\%$ and $5\,wt\,\% \leqslant y \leqslant 15\,wt\,\%$) has systematically been studied by the dilatometry technique. Different techniques of analysis such as X-ray diffraction (XRD), optical microscopy and electron probe microanalysis (EPMA) were then used to identify phases obtained at different temperatures.

3. Dilatometric trials

Dilatometric curves recorded during the sintering cycle from different agglomerates (Fig. 1) permit the following observations. The shrinkage of compacts starts, in all cases, at about 540 °C, probably in relation to the establishment of "necks" between the iron particles contained in the mixtures [15, 16]. Afterwards, a perturbing expansion is observed, on the different curves, at about 620 °C. A similar phenomenon has been observed during the sintering of different powder mixtures as a consequence of the Kirkendall effect [17–19]. Another perturbing expansion is observed on the dilatometric curves at ~ 890 °C. The amplitude of this latter expansion increases remarkably as a function of molybdenum content. On the contrary, the shrinkage starts again, after this expansion, at a temperature which decreases as a function of molybdenum addition. Similar expansions have also been observed during the sintering of both Fe–W [20] and Fe–Mo [21] systems in relation to Fe_2W and Fe_7Mo_6 formation, respectively, whereas the origin of the expansion observed in the case of the Fe–W–Mo ternary systems is the formation of a ternary intermetallic compound with Fe_7M_6 stoichiometry [22]. A third expansion is observed on curves corresponding to compacts with high percentages of tungsten. Nevertheless, the expansion related to this phenomenon is not so important as that observed at ~890 °C. Moreover, it decreases rapidly when the added percentage of molybdenum is increased.

Those parts of the dilatometric curves recorded during the cooling of the samples show two anomalies (similar to those observed in the Fe–Mo [23] binary system). The first anomaly corresponding to a compression of compacts, occurred at high temperature (beyond 1180 °C). This may be due to the precipitation of Fe_7M_6 ternary intermetallic compound [22] (where M is tungsten and molybdenum). The second anomaly, corresponding to an expansion of agglomerates, occurred below 800 °C as a consequence of Fe_2M intermetallic compound precipitation.

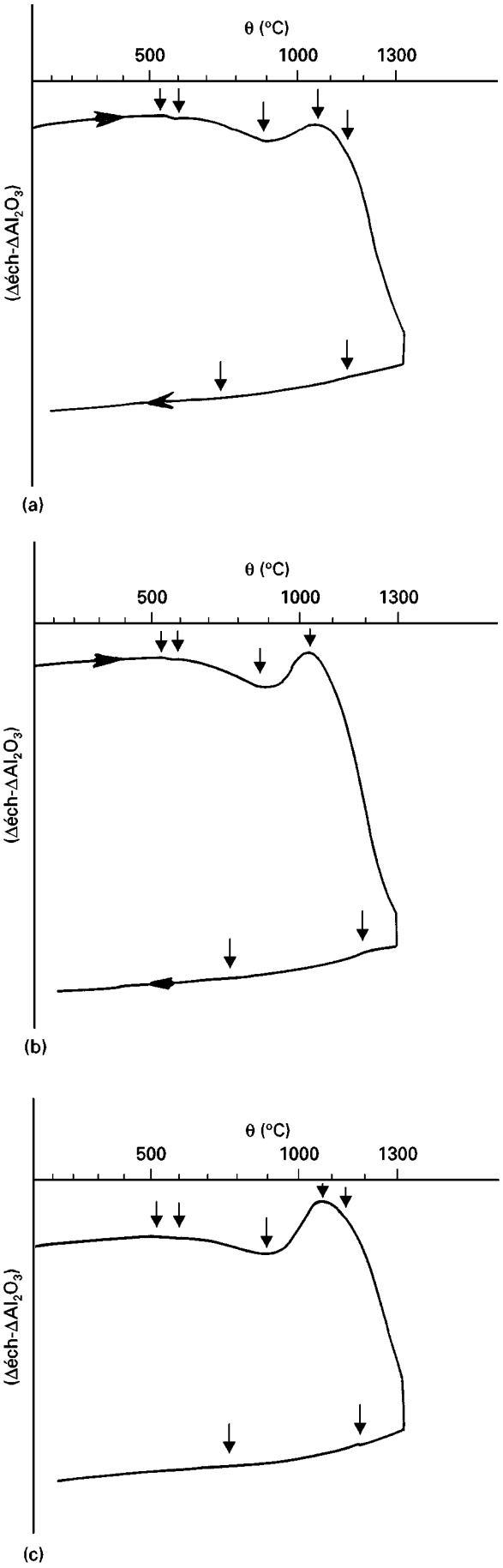

Figure 1 Dilatometric curves recorded from different samples during the sintering treatment: (a) Fe–15 wt % W–5 wt % Mo; (b) Fe–15 wt % W–10 wt % Mo; (c) Fe–15 wt % W–15 wt % Mo.

4. Evolution of compact shrinkage at different temperatures

The curves shown in Figs 2–4 illustrate the shrinkage undergone by different Fe–W–Mo compacts within different temperature ranges, as a function of tungsten and molybdenum weight percentages. The shrinkage

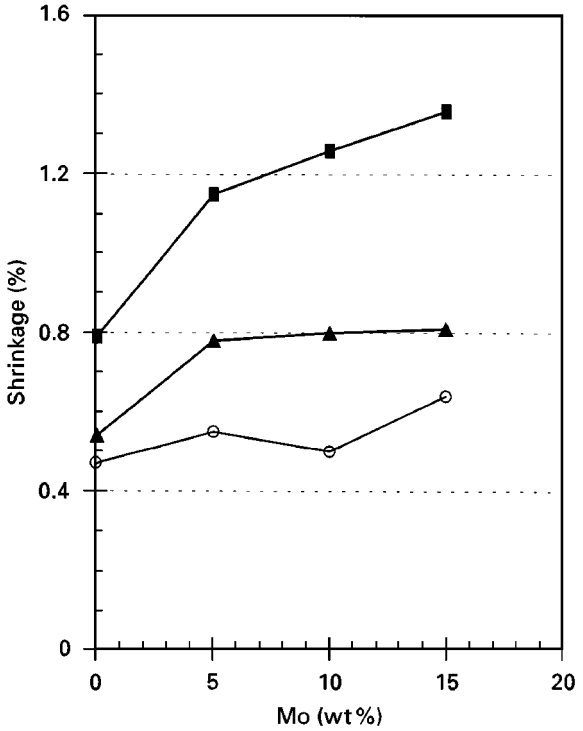

Figure 2 Shrinkage of compacts between room temperature and 900 °C as a function of molybdenum percentage for different total additions: (■) 20 wt %, (▲) 25 wt %, (○) 30 wt %.

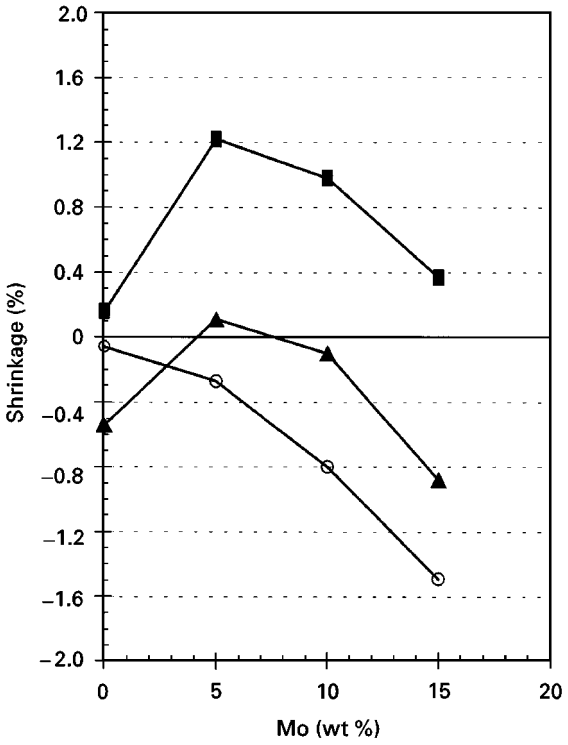

Figure 3 Shrinkage of compacts between 900 and 1100 °C as a function of molybdenum percentage for different total additions: (■) 20 wt %, (▲) 25 wt %, (○) 30 wt %.

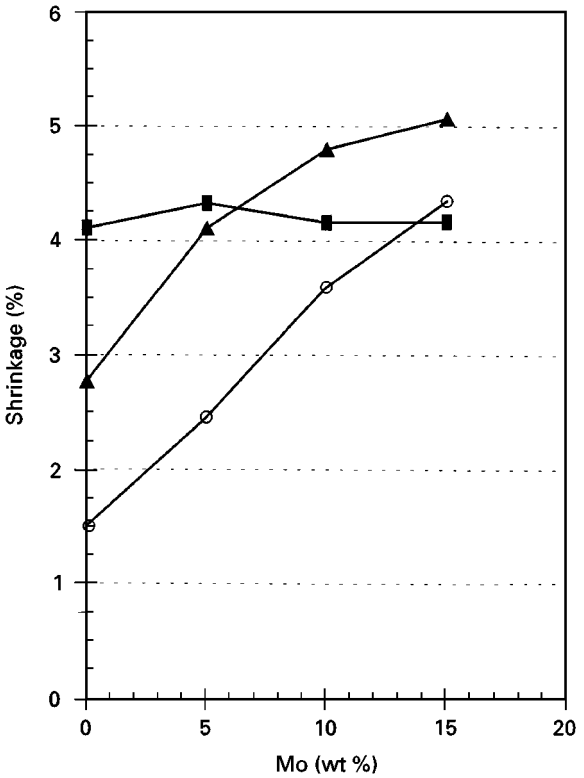

Figure 4 Shrinkage of compacts between 1100 and 1300 °C as a function of molybdenum percentage for different total additions: (■) 20 wt %, (▲) 25 wt %, (○) 30 wt %.

values were determined from dilatometric curves as proposed by Tolba-Sallam [24]. It can be noticed that the shrinkage undergone by samples between 20 and 900 °C (Fig. 2), decreases as a function of the total percentage of tungsten and molybdenum. Such behaviour may be attributed to the fact that the shrinkage of similar systems, within this temperature range is mainly controlled by iron particle welding. When tungsten and molybdenum additions are increased, the fraction of iron particles in the samples diminishes and consequently leads to a decrease in shrinkage. On the other hand, Fig. 2 reveals an advantageous effect of molybdenum addition on the shrinkage. This is probably due to a better interdiffusion between molybdenum and iron within this temperature range, in comparison to the interdiffusion between tungsten and iron.

Fig. 3 shows a similar evolution of the shrinkage between 900 and 1100 °C as a function of the total percentage of molybdenum and tungsten. But, the effect of molybdenum addition on the shrinkage is obviously different from that observed within the previous temperature range. Indeed, an advantageous effect of molybdenum on the shrinkage is observed up to 5 wt % (for samples containing 20 and 25 wt % Mo and W total percentage). On the contrary, for molybdenum percentages higher than 5 wt %, this element inhibits the shrinkage acquired between 900 and 1100 °C. To explain this shrinkage evolution, it should be noticed that interdiffusion between iron, molybdenum and tungsten leads to two opposite effects. Firstly, the diffusion of molybdenum and tungsten atoms in the iron lattice inhibits the growth of the

$(Fe–M)_\alpha$ solid solution grains. By this fact, the shrinkage increases owing to the elimination of the pores by the $(Fe–M)_\alpha$ grain boundaries. Secondly, the difference between the diffusion coefficients of iron, tungsten and molybdenum induces a Kirkendall effect which leads to an expansion of the samples. In the case of samples containing 20 and 25 wt % of the total percentage, the effect of grain refinement on the shrinkage may be more important than the Kirkendall effect up to 5 wt % Mo. Therefore, an increase in shrinkage as a function of molybdenum content is observed. On the other hand, the Kirkendall effect becomes predominant in the other cases. Consequently, the shrinkage diminishes with increasing molybdenum addition.

The curves corresponding to the shrinkage acquired by agglomerates between 1100 and 1300 °C (Fig. 4) permit the following conclusions. The shrinkage decreases as a function of the total percentage of tungsten and molybdenum. On the other hand, an increase in molybdenum percentage is generally conducive to an improvement of the shrinkage within this temperature range. But, a feeble effect of molybdenum on the shrinkage produced between 1100 and 1300 °C is observed in the case of samples containing 20 wt % of the total percentage. This behaviour may also be related to different factors which have opposite effects on the shrinkage. The principals are the formation of the intermetallic compound and the increase in both molybdenum and tungsten solubility in the Fe_α lattice at high temperature. As it has been mentioned above that the formation of the intermetallic compound is accompanied by the appearance of a secondary porosity which inhibits the shrinkage. In this fashion, this factor tends to decrease the shrinkage when the total addition of molybdenum and tungsten is increased. By contrast, the increase of molybdenum and tungsten solubility in the Fe_α lattice, at high temperature, rather tends to increase the shrinkage. It should be noticed, furthermore, that the solubility of molybdenum in Fe_α is more important than that of tungsten, so its influence on increasing shrinkage is more marked. This fact explains, in particular, why the shrinkage increases as a function of molybdenum percentage in the case of samples containing the same total addition. In the case of a sample containing 20 wt %, the effect of the two factors are counterbalanced, therefore molybdenum addition slightly influences the shrinkage evolution within this temperature range.

5. X-ray diffraction analysis

X-ray spectra recorded from different sintered samples (Fig. 5) reveal principally lines of (b c c) $(Fe–M)_\alpha$ solid solutions. In the case of agglomerates containing high tungsten and molybdenum percentages (Fig. 5b and c) additional lines corresponding to the ternary Fe_7M_6 intermetallic compounds are also observed.

On the other hand, Fig. 6 shows the variation of the lattice parameter of $(Fe–M)_\alpha$ solid solutions, obtained in different sintered samples, with tungsten and molybdenum additions. It can be noticed that the lattice parameter varies insignificantly with both tungsten and molybdenum percentages. The corresponding values were, furthermore, about 0.2884 nm for all studied samples. Two conclusions may be drawn from these results. Firstly, the $(Fe–M)_\alpha$ solid solutions obtained after sintering in these samples are probably saturated with tungsten and molybdenum elements. For this reason, the lattice parameter is not affected by the initial percentages of tungsten and molybdenum in

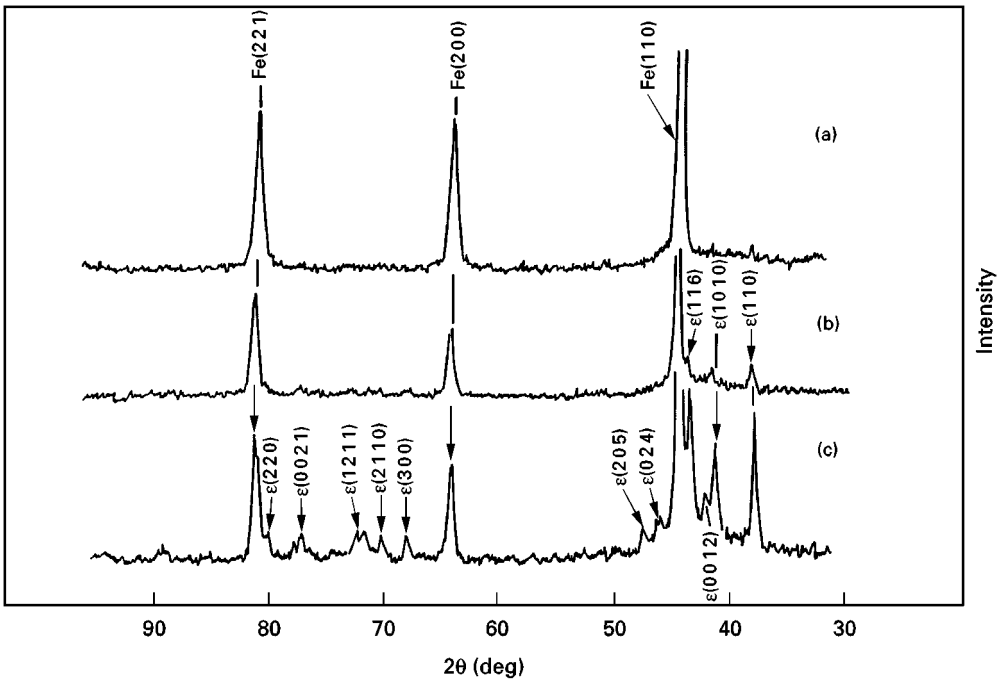

Figure 5 X-ray spectra recorded from different (Fe–W–Mo) samples sintered at 1300 °C for 10 min: (a) Fe–15 wt % W–5 wt % Mo; (b) Fe–15 wt % W–10 wt % Mo; (c) Fe–15 wt % W–15 wt % Mo.

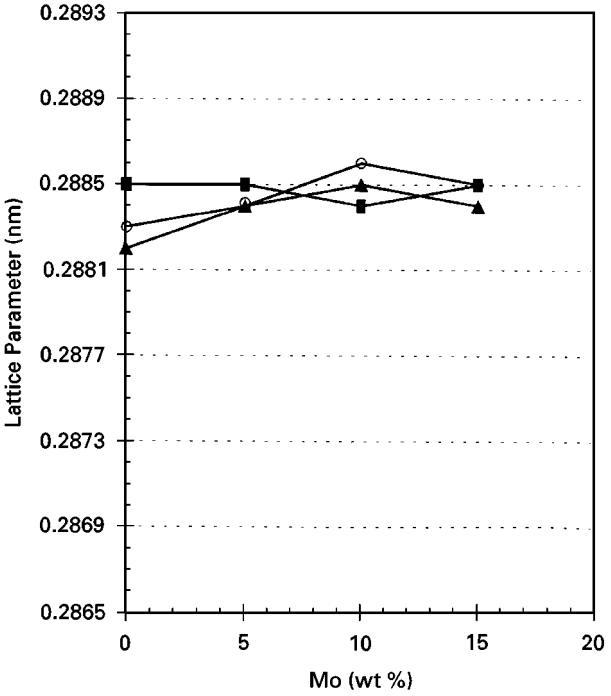

Figure 6 Evolution of $(Fe–M)_\alpha$ solid solution lattice parameter as a function of molybdenum percentage for different total additions: (■) 20 wt %, (▲) 25 wt %, (○) 30 wt %.

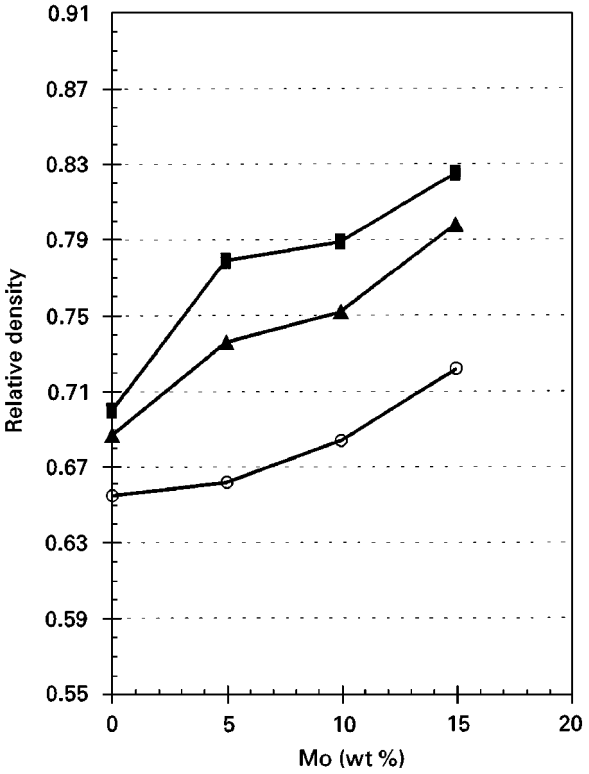

Figure 7 Relative density of different (Fe–W–Mo) sintered samples as a function of molybdenum percentage for different total additions: (■) 20 wt %, (▲) 25 wt %, (○) 30 wt %.

the agglomerates. Secondly, the $(Fe–M)_\alpha$ solid solutions obtained after sintering probably correspond to that formed at higher temperatures. The corresponding lattice parameters are effectively too great to be attributed to $(Fe–M)_\alpha$ solid solutions formed at room temperature. For example, the tungsten atomic percentage of the solid solutions obtained in the Fe–25 wt % W sample was estimated to be about 5 at % by Vegard's law. But, according to the (Fe–W) phase diagram, this value is greater than the solubility limit of tungsten in an iron lattice at room temperature.

6. Density and microhardness of the sintered samples

The final density of the sintered samples is affected by both tungsten and molybdenum additions. Fig. 7 shows that the relative density (the ratio of the sintered sample density to the theoretical density) of the sintered samples decreases when the total percentage of molybdenum and tungsten is increased. Besides, the relative density of samples containing the same total percentage is the higher than when the molybdenum addition is increased. This result may confirm the beneficial effect of molybdenum on the sintering of such systems.

Furthermore, microhardness tests performed on different sintered samples (Fig. 8) reveal an increase in the $(Fe–M)_\alpha$ solid solutions microhardness as a function of both tungsten and molybdenum additions in the case of samples containing up to 10 wt% Mo addition. On the contrary, the $(Fe–M)_\alpha$ solid solution microhardness varies slightly with tungsten addition but increases as a function of molybdenum percentage in the case of higher molybdenum addition (>10 wt %). This latter result probably reflects the

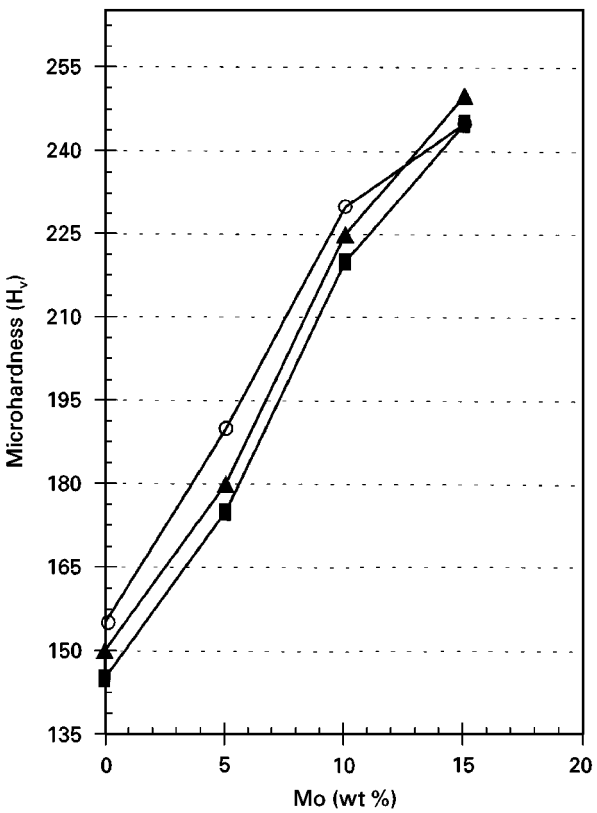

Figure 8 Evolution of $(Fe–M)_\alpha$ solid solution microhardness as a function of molybdenum percentage for different total additions: (■) 20 wt %, (▲) 25 wt %, (○) 30 wt %.

substitution of a certain proportion of tungsten atoms in the solid solutions by a greater proportion of molybdenum atoms when the initial percentage of molybdenum is increased.

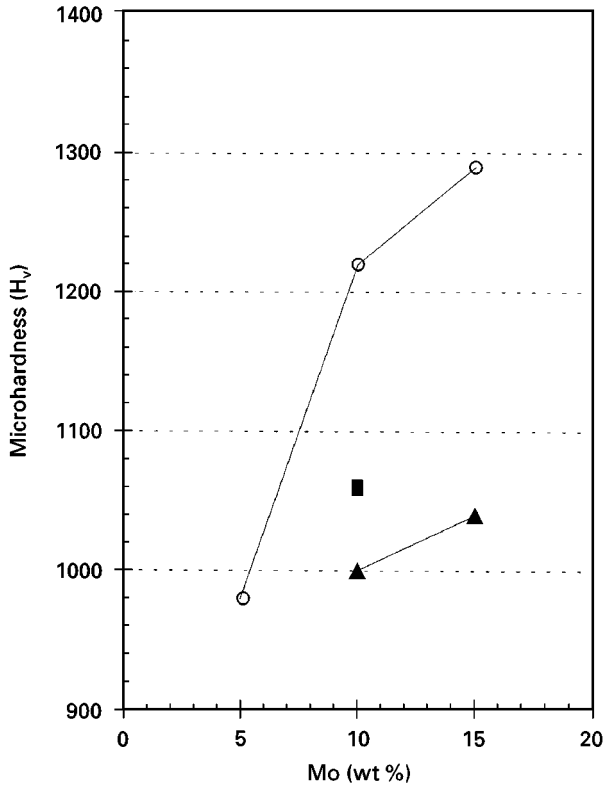

Figure 9 Evolution of intermetallic compounds microhardness with molybdenum initial percentage in samples for different total additions: (■) 20 wt %, (▲) 25 wt %, (○) 30 wt %.

On the other hand, microhardness tests carried out on intermetallic compounds obtained for different sintered samples show a great dispersion of the measured values which varies between 1000 and 1300 H_v. However, the curves illustrated in Fig. 9, show an increase in the average microhardness of the intermetallic compounds as a function of molybdenum percentage. The origin of this evolution may be related to the variation of the intermetallic compound chemical composition versus the initial tungsten and molybdenum additions [22].

7. Microstructure of the sintered samples

All micrographs in Fig. 10 confirm the presence of $(Fe–M)_\alpha$ solid solutions and intermetallic compounds in the sintered samples. Additionally, several remarks can be drawn from these micrographs. The residual porosity in the sintered samples is more important than a higher total percentage of tungsten and molybdenum. The obtained pores are irregularly shaped and are generally localized near the intermetallic compounds. However, for the same total addition, the porosity diminishes when the molybdenum percentage is increased. Besides, increasing the molybdenum addition is conducive to evolution of both morphology and volume proportion of the intermetallic compounds. The volume fraction of the intermetallic compounds increases at the same time as the molybdenum percentage is increased. Finally, the same micrographs permit the presence of a certain proportion of intermetallic compounds to be noted along solid solution grain boundaries.

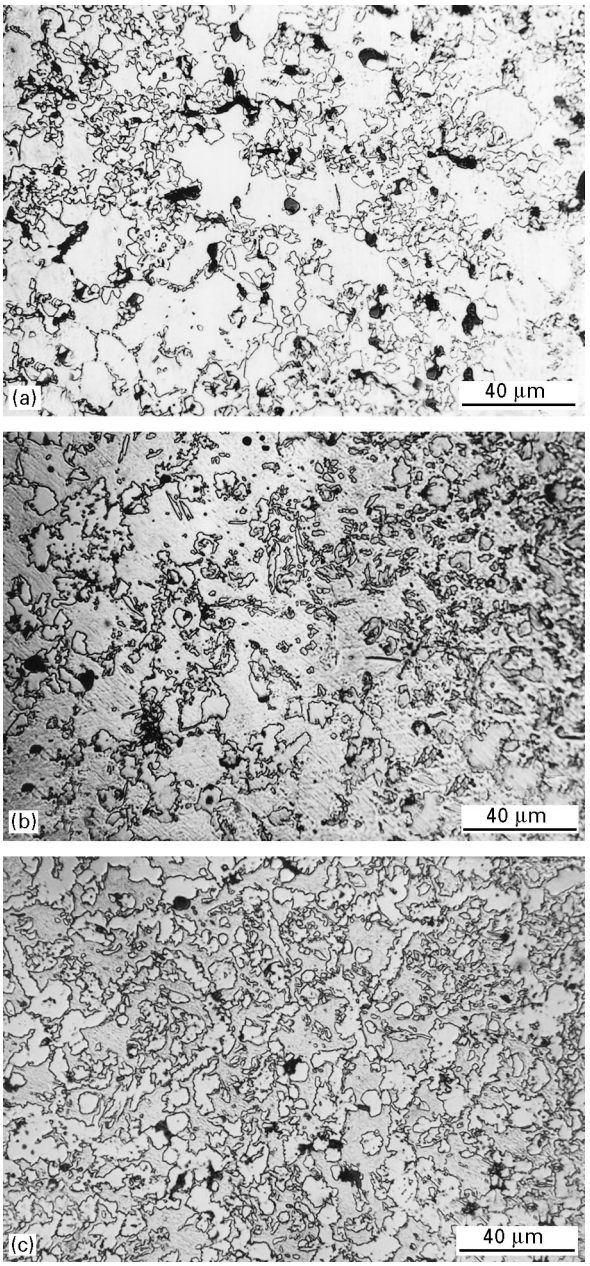

Figure 10 Microstructure of different (Fe–W–Mo) samples sintered at 1300 °C for 10 min: (a) Fe–25 wt % W–5 wt % Mo; (b) Fe–15 wt % W–10 wt % Mo; (c) Fe–15 wt % W–15 wt % Mo.

This fact may reflect their precipitation during sample cooling.

8. Evolution of sample structure during the sintering treatment

In order to clarify the structure evolution of agglomerates during the sintering treatment, parts of the X-ray spectra were recorded between 35° and 45° (2θ diffraction angle), using a slow rotating speed of the sample holder, from Fe–15 wt % W–15 wt % Mo samples sintered at different temperatures for 2 h. The X-ray spectrum recorded from the sample sintered at 620 °C (Fig. 11a) reveals only lines corresponding to Fe_α, molybdenum and tungsten elements. However, a shift of the (1 1 0) Fe_α line to lower diffraction angles (in comparison with that corresponding to pure iron) is observed. This reflects the formation of $(Fe–M)_\alpha$ solid

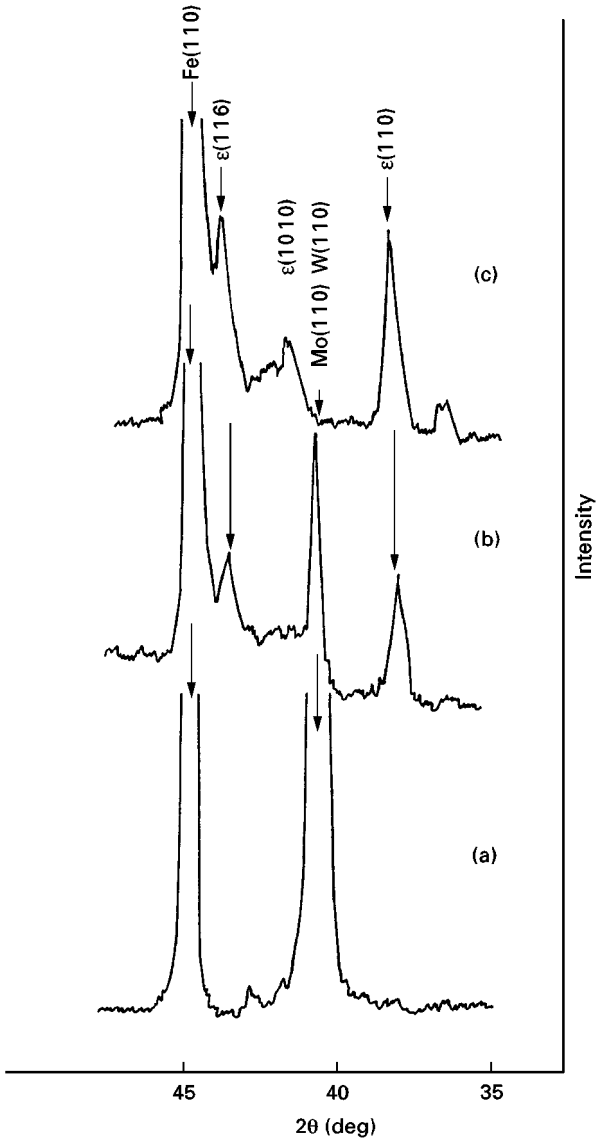

Figure 11 X-ray spectra recorded from Fe–15 wt % W-15 wt % Mo samples sintered at different temperatures for 2 h: (a) 620 °C; (b) 900 °C; (c) 1100 °C.

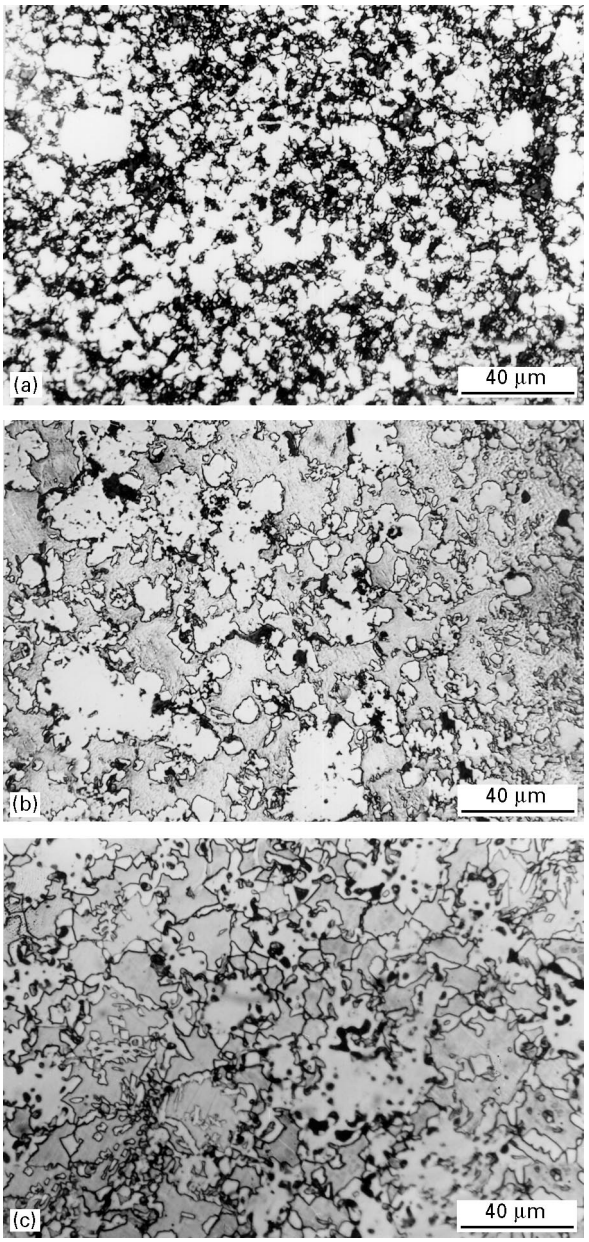

Figure 12 Microstructure of Fe–15 wt % W–15 wt % Mo samples sintered at different temperatures for 2 h: (a) 620 °C; (b) 900 °C; (c) 1100 °C.

solutions in the compact at this temperature. On the other hand, the micrograph corresponding to the same sample (Fig. 12a) shows essentially the starting particles, but the beginning of welding between some of these particles is observed. Therefore, it can be concluded that a certain interdiffusion already occurs between iron, molybdenum and tungsten within this temperature range. The difference between the diffusion coefficients corresponding to the three elements is probably conducive to a Smigelskas–Kirkendall effect which is the origin of the expansion observed at about 620 °C on the dilatometric curves.

The X-ray spectrum realized from the sample sintered at 900 °C (Fig. 11b) reveals a notable diminution of the (1 1 0) line intensity corresponding to molybdenum and tungsten phases. By contrast, the intensity of the (1 1 0) line corresponding to $(Fe–M)_\alpha$ solid solution is somewhat affected by the sintering temperature. These results may evince an increase in molybdenum and tungsten diffusion in the α-iron lattice at this temperature. In addition, the same X-ray spectrum reveals the presence of lines corresponding to Fe_7M_6 intermetallic compound confirming, by this fact, the formation of this intermetallic compound at about 900 °C. On the other hand, the structure of the sample (Fig. 12b), is mainly constituted of large domains of $(Fe–M)_\alpha$ solid solutions (brown regions) and areas of undiffused molybdenum and tungsten (relatively bright regions). It can also be noticed that some areas are larger than the molybdenum and tungsten starting particles. This means that they have probably been formed as a consequence of the welding between molybdenum and tungsten starting particles. Another important point to note in this case is the appearance of irregularly shaped pores localized at borders of the molybdenum and tungsten undiffused areas. At the same time, small precipitates of Fe_7M_6 intermetallic compound are observed throughout $(Fe–M)_\alpha$ solid solutions. These observations confirm, the correlation between the appearance of this intermetallic compound and the

expansion observed at about 890 °C on the dilatometric curves.

Finally, the X-ray spectrum corresponding to the Fe–15 wt % W–15 wt % Mo sample sintered at 1100 °C (Fig. 11c) reveals an increase in the line intensities of the intermetallic compound, while the (1 1 0) line corresponding to molybdenum and tungsten phases disappears completely. The corresponding micrograph (Fig. 12c) shows particularly the growth of the intermetallic compound precipitates at the $(Fe–M)_\alpha$ solid solution grain boundaries. An important porosity, constituted essentially of large and irregularly shaped pores, can also be observed at the borders of the undiffused molybdenum and tungsten areas. These observations support the idea that such porosity appears as a consequence of an enhancement of tungsten diffusion from undiffused areas to the intermetallic compounds and $(Fe–M)_\alpha$ solid solutions at high temperature.

Furthermore, Fig. 13 illustrates the evolution of both diffraction angle and intensity corresponding to the (2 1 1) line of $(Fe–M)_\alpha$ solid solutions with sintering temperature. A shift of the line to the lower diffraction angles is observed when the sintering temperature is increased, whilst the width of the peak increases. This confirms the formation of solid solutions richer in tungsten and molybdenum as the sintering temperature increases, but, at the same time, the chemical homogeneity of the solid solutions diminishes.

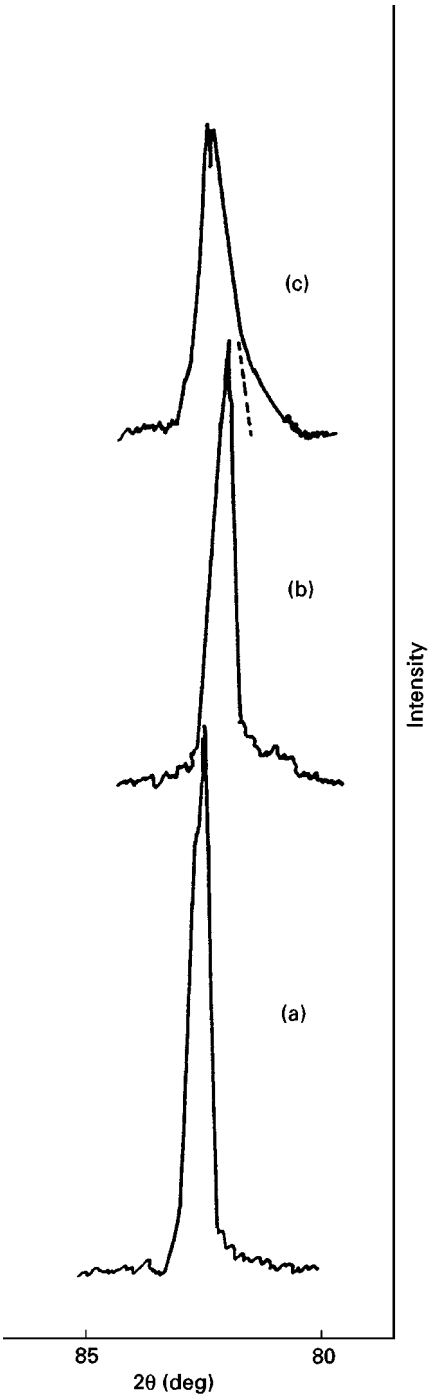

Figure 13 Evolution of the $(Fe–M)_\alpha$ solid solutions (2 1 1) diffraction line, recorded from Fe–15 wt % W–15 wt % Mo samples, with the sintering temperature: (a) 620 °C; (b) 900 °C; (c) 1100 °C.

9. Electron microprobe analysis

Electron probe microanalysis was performed on Fe–10 wt % W–10 wt % Mo samples sintered at different temperatures for 3 days. Table I, gives average weight percentages of iron, molybdenum and tungsten obtained by analysis, carried out at five different sites throughout matrices of agglomerates held at different temperatures. The obtained results confirm that the matrix is constituted, in all cases, of solid solutions of both molybdenum and tungsten in Fe_α lattice. It can be noticed, at the same time, that the molybdenum percentage is somewhat higher than that of tungsten, in solid solutions formed at 800 °C as well as that formed at 930 °C owing to the higher interdiffusion between iron and molybdenum in comparison with that between iron and tungsten in this temperature range. On the contrary, the tungsten percentage in $(Fe–M)_\alpha$ solid solutions becomes of the same order of magnitude as that of molybdenum in the case of a sample heat treated at 1200 °C. So, it can be concluded that tungsten diffusion in $(Fe–M)_\alpha$ solid solution increases appreciably at high temperature.

Furthermore, analysis carried out on intermetallic compounds formed at different temperatures [22] have also shown, a particular increase in tungsten percentage of the intermetallic compounds formed at 1200 °C. These results corroborate the hypothesis made above concerning an enhancement of tungsten diffusion in the intermetallic compounds at high temperature. This phenomenon leads to the appearance of a noticeable secondary porosity, where the pores are localized near the intermetallic compound precipitates (Fig. 14).

10. Evolution of sintered samples during a second cycle of heat treatments

The dilatometric curves shown in Fig. 15 were recorded during a second cycle of heat treatment on samples presintered at 1300 °C for 10 min. Those parts of the curves realized during the heating show the following evolution.

A compression of samples is noticed between 700 and 900 °C which probably reflects the dissolution of the Fe_2M intermetallic compounds in $(Fe–M)_\alpha$ solid

TABLE I Results of analysis carried out on matrices of Fe + 10Mo + 10W samples sintered at different temperatures for 3 days

Analysis	800 °C			930 °C			1200 °C		
	Fe	Mo	W	Fe	Mo	W	Fe	Mo	W
1	92.89	3.98	1.93	90.92	5.63	2.66	81.98	8.07	7.25
2	93.21	3.39	3.45	91.20	5.56	2.75	81.73	8.01	6.87
3	90.82	4.86	3.55	90.72	5.38	3.46	82.11	7.60	7.02
4	94.06	3.76	1.86	91.76	5.88	3.02	77.53	9.53	8.31
5	93.28	3.41	1.41	92.73	5.30	3.20	82.78	7.80	6.90

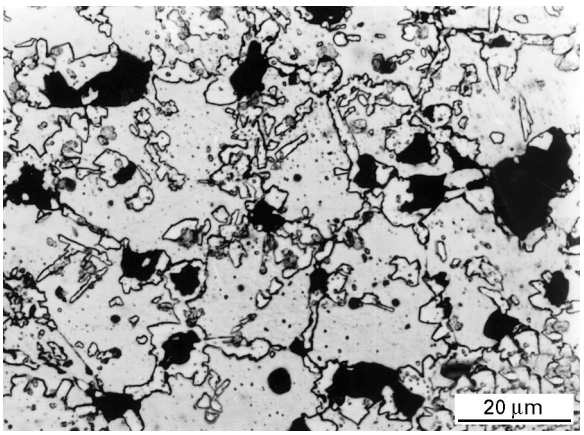

Figure 14 Micrograph of Fe–15 wt % W–15 wt % Mo sintered at 1300 °C for 10 min.

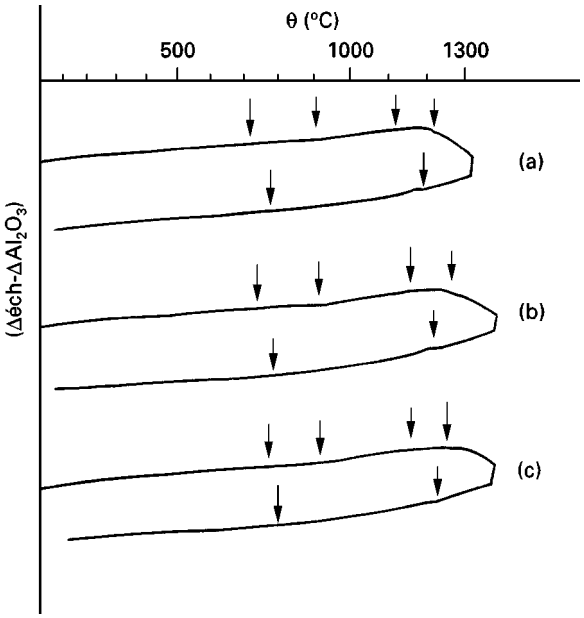

Figure 15 Dilatometric curves recorded from different presintered samples during a second cycle of heat treatment: (a) Fe–20 wt % W–10 wt % Mo; (b) Fe–15 wt % W–15 wt % Mo; (c) Fe–25 wt % W–5 wt % Mo.

solution grains. On the other hand, the dissolution of the Fe_7M_6 intermetallic compounds in $(Fe–M)_\alpha$ solid solutions generates, for its part, an expansion of samples between 900 and 1100 °C. Afterwards, an onset of shrinkage is observed on the dilatometric curves at a temperature which increases as a function of the initial molybdenum percentage in the sample. This behaviour can be explained by the fact that samples containing a higher percentage of molybdenum reach a higher density after the first sintering cycle. At high temperatures, the curves show a perturbing expansion linked to the Kirkendall effect which appears as a consequence of the increase in tungsten diffusion from undiffused areas of the intermetallic compounds. This phenomenon is shifted to higher temperatures when the percentage of molybdenum in the sample is increased, owing to the higher homogeneity of samples obtained after the first cycle. Those parts of the curves recorded during cooling show two anomalies, corresponding to the precipitation of the Fe_7M_6 and Fe_2M intermetallic compounds, respectively. The precipitation of the first compound occurs at about 1200 °C in the case of the Fe–25 wt % W–5 wt % Mo, but increases steadily with molybdenum percentage. This result first shows that these samples evolve in the $(Fe–M)_\alpha$ solid solution domain at high temperature, and secondly that the solubility of the total percentage of molybdenum and tungsten in $(Fe–M)_\alpha$ solid solution grains increases as a function of the added percentage of molybdenum. The precipitation of the second compound occurs at about 800 °C and varies insignificantly with the added percentages of both molybdenum and tungsten, because the considered samples evolve, within this range of temperature, in a bi-phase domain independently of their chemical compositions.

11. Conclusion

The evolution of Fe–W–Mo ternary agglomerates prepared from mixtures of iron, tungsten and molybdenum powders is characterized by an onset of shrinkage at about 540 °C as a consequence of the establishment of "necks" between iron particles contained in mixtures. Subsequently, the sintering is inhibited by three perturbing expansions. The first appears at about 620 °C following the development of a Kirkendall effect as a consequence of the difference between the diffusion coefficients of iron, molybdenum and tungsten. The second expansion, whose amplitude is more important, appears at about 890 °C and is attributed to the formation of a ternary intermetallic compound with Fe_7M_6 stoichiometry. The third expansion appears at about 1200 °C in correlation with an enhancement of the tungsten diffusion in intermetallic compounds and $(Fe–M)_\alpha$ solid solutions which simultaneously leads to an important Kirkendall effect.

During cooling of the compacts, a ternary intermetallic compound, Fe_7M_6, precipitates at high temperature (above 1100 °C), while a Fe_2M compound precipitates at lower temperature (below 800 °C). As a consequence of this evolution, the structure of the sintered samples was mainly constituted of hard intermetallic compounds dispersed throughout the $(Fe–M)_\alpha$ matrix. At the same time, the retained porosity which increases with the total added percentage of tungsten and molybdenum was observed in the sintered samples. The results obtained also show that molybdenum enhances the sintering of the

agglomerates and by this fact is conducive to an increase in both final density and microhardness of the obtained samples. It has been found that molybdenum addition also affects both chemical composition and microhardness of the intermetallic compound formed in these samples.

References

1. A. JENKINS, *Powder Metall.* **24** (1969) 503.
2. F. L. CARLSEN, J. R. DREYERS and D. G. DREYERS, *Int. J. Powder Metall.* **4** (1968) 31.
3. G. DESPLANCHES, Colloque "Nouvelles Poudres, Nouveaux Produits en Métallurgie des Poudres et Céramiques spéciales", (Groupe Français de la Céramique et Société Française de Métallurgie, Paris, 1988) p. 19.1.
4. Ph. DUBOIS, L. THEMELIN and G. P. BRUNEL, *ibid*., p. 13.1.
5. M. M. REBBECK, J. D. BOLTON and M. LEWICKA-SHAFER, in "Proceedings of the World Conference on Sintering", London, Vol. 1 (The Institute of Metals, London, 1990) p. 196.
6. F. THUMMLER and C. GUTSFELD, *ibid*., Vol. 1, p. 25.
7. G. P. BRUNEL, Ph. DUBOIS and L. THEMELIN, *ibid*., Vol. 2, p. 333.
8. J. D. BOLTON, Colloque "Nouvelles Poudres, Nouveaux Produits en Métallurgic des Poudres et Céramiques spéciales", (Groupe Français de la Céramique et Société Française de Métallurgie, Paris, 1988) p. 15.1.
9. J. M. MARTINS, M. M. OLIVEIRA and H. CARVALHINHOS, *ibid*., p. 16.1
10. N. KAWAI and H. TAKIGAWA, *Metal Powder Rep.* **38** (1982) 237.
11. C. S. WRIGHT and L. FONTAINE, Colloque "Nouvelles Poudres, Nouveaux Produits en Métallurgie de Poudres et Céramiques spéciales", (Groupe Français de la Céramique et Société Française de Métallurgie, Paris, 1988) p. 22.1
12. G. GREETHAM, in "Proceedings of the World Conference on Sintering", London, Vol. 1 (The Institute of Metals, London, 1990) p. 206.
13. D. T. HAWKINS and R. HULTGRIN, "Metals Hand Book", (8th Edn, American Society for Metals, Ohio, 1973) Vol. VIII, p. 303.
14. *Idem*., *ibid*., p. 307.
15. G. CIZERON, thèse de Docteur Ingénieur, Paris XI (1957).
16. F. J. ESPER, H. E. EXNER and H. METZLER, *Powder Metall.* **35** (1975) 107.
17. D. GEORGEAULT, R. DESSIEUX and G. CIZERON, *Ann. Chim. Sci. Matér.* **6** (1982) 483.
18. M. TOLBA-SALLAM, G. HENRY and G. CIZERON, *Mét. Corros. Ind.* **56** (1981) 161.
19. B. L. MASSON and G. CIZERON, *Powder Metall.* **4** (1991) 285.
20. C. SERVANT, thése de 3éme Cycle, ParisXI (1967).
21. A. BOULAMA, G. P. BRUNEL and G. CIZERON, in "Proceedings of the World Conference on Sintering", Vol. 2 (The Institute of Metals, London, 1990) p. 222.
22. S. E. BARAMA, A. HARABI, G. CIZERON, *J. Mater. Sci. Lett*. **16** (1996) 1240.
23. A. BOULAMA, thèse de Docteur en Sciences, Paris XI (1994).
24. M. TOLBA-SALLAM, thèse de Docteur Ingénieur, Paris XI (1981).

Received 21 October 1996
and accepted 27 January 1998